Chemical Science

ROYAL SOCIETY OF CHEMISTRY

EDGE ARTICLE

View Article Online
View Journal | View Issue

Cite this: *Chem. Sci.*, 2025, **16**, 17207

All publication charges for this article have been paid for by the Royal Society of Chemistry

Received 15th May 2025
Accepted 14th August 2025

DOI: 10.1039/d5sc03501e

rsc.li/chemical-science

From $NaSc_3Ga_2Q_8$ (Q = S, Se) to $KGa_2In_3S_8$: substitution of Sc^{3+} with In^{3+} to achieve doubled birefringence

Yun Xie,[a] Wen-Dong Yao,*[a] Qiu-Yang Du,[a] Wenfeng Zhou,[a] Nian-Tzu Suen,[a] Wenlong Liu[a] and Sheng-Ping Guo *[ab]

The exploration of novel compounds with new crystal and electronic structures is essential for advancing the development of functional materials. Here, three novel isomorphic quaternary alkali-metal chalcogenides, AM_5Q_8 (A = Na, K; M = Sc, Ga and In; Q = S, Se), with a new structure type have been obtained by a facile reactive flux assisted boron–chalcogen solid-state method, and adopt a 3*D* $\{[M_5Q_8]^-\}_\infty$ open-framework architecture with A^+ ions occupying the cavities to balance charges. Subtle modulation of the M–Q bonds induces a twofold enhancement in optical birefringence (Δn), observed from $NaSc_3Ga_2Q_8$ (Q = S, Δn = 0.050@532 nm; Q = Se, Δn = 0.088@532 nm) to $KGa_2In_3S_8$ (Δn = 0.134@532 nm). Their optical band gaps are 2.21–3.10 eV. The theoretical calculation results reveal that the replacement of Sc with In enhances the orbital hybridization between cations and anions, amplifies microscopic polarizability anisotropy and consequently doubles the birefringence. In addition, $KGa_2In_3S_8$ exhibits a photocurrent density of ~30 nA cm^{-2}. This work provides novel insights for improving the birefringence performance of materials.

Introduction

Inorganic multinary metal chalcogenides, with their diversity of crystal structures and tunable electronic structures, have been a focus of condensed matter physics and materials chemistry in the development of novel materials in the fields of nonlinear optics (NLO),[1,2] photoluminescence,[3–5] magnetism,[6,7] thermoelectricity,[8–10] superconductivity,[11,12] and energy storage and conversion.[13,14]

In recent years, ternary chalcogenides AM_5Q_8 (A = alkali metal, Tl and Ag; M = trivalent transition metal, Ga, In and Sb; Q = S, Se and Te) with rich site-regulated structures have shown excellent performances in various fields. Members of this family crystallizing in the centrosymmetric (CS) space group *C*2/*m* generally exhibit characteristic 3*D* tunneling framework structures, and have been reported to exhibit magnetic and thermoelectric properties, including ACr_5Te_8 (A = K, Cs and Rb),[15] $RbSc_5Te_8$,[16] $CsTi_5S_8$,[17] and TlV_5S_8.[18] Such structures can be traced back to *Hollandite* $A_xM_8O_{16}$, where the A-site cations (alkali or alkaline-earth metal) occupy tunnels, and the M-site cations (transition metal) construct a continuous tunneling network through sharing O-corners and edges with the BO_6 octahedra.[19] Similar to *Hollandite* materials, such compounds are stoichiometrically flexible and their properties can be optimized by adjusting the A-site ion occupancy, such as $Rb_xCr_5Te_8$ (x = 0.73 and 0.62),[20] $Cs_xCr_5Te_8$ (x = 0.73, 0.91 and 0.97)[21] and $Tl(V_{1-x}Cr_x)_5Se_8$ (x = 0–1 and Δx = 0.2).[22] Some other AM_5Q_8 members crystallize in noncentrosymmetric (NCS) space groups, like $AgIn_5Se_8$ ($P4\bar{2}m$),[23] AGa_5S_8 (A = K, Rb and Cs; $P2_1$ or *Iba*2),[24] α-KGa_5Se_8 ($P2_1$),[25] β-KGa_5Se_8 ($P1$),[25] and ASb_5S_8 (A = K and Rb; *Pn*).[26,27] Besides, $CsSb_5S_8$ crystallizes in the CS space group $P2_1/n$.[27] They are all composed of MQ_4 (M = In, Ga and Sb; Q = S and Se) units forming sub-structural motifs *via* corner- or edge-sharing, and the difference among them is that AGa_5S_8 (A = K, Rb, and Cs), α-KGa_5Se_8, and β-KGa_5Se_8 have similar 3*D* honeycomb $\{[Ga_5Q_8]^-\}_\infty$ framework structures, whereas the layered structures of ASb_5S_8 (A = K and Rb) are more clearly characterized, and $AgIn_5Se_8$ exhibits a defect diamond-like structure. These compounds show outstanding NLO properties; particularly, β-KGa_5Se_8 demonstrates enhanced birefringence Δn and achieves phase-matching with a 1910 nm laser.

Interestingly, AM_5Q_8 members crystallizing in the CS space group *C*2/*m* feature MQ_6 octahedra as their only basic structural unit, which are transformed into MQ_4 tetrahedra when the structure is converted to the NCS one. The AM_5Q_8 compounds, particularly those with NCS structures, exhibit obvious cation substitution effects, and slight changes in bond lengths may trigger significant differences in band structure, optical anisotropy, and even crystal symmetry. Our recently discovered $CsScP_2S_7$ exhibits promising NLO properties.[28] Compared to

[a]*School of Chemistry and Chemical Engineering, Yangzhou University, Yangzhou 225002, P. R. China. E-mail: wdyao_sora@163.com*

[b]*Yunnan Key Laboratory of Electromagnetic Materials and Devices, National Center for International Research on Photoelectric and Energy Materials, School of Materials and Energy, Yunnan University, Kunming 650500, P. R. China. E-mail: spguo@yzu.edu.cn*

other trivalent cations, ScS_6 octahedra exhibiting d^0-driven subtle Jahn–Teller distortions break structural symmetry, synergized with the deep level 3d orbital characteristics, and enhance the second harmonic response while maintaining a high laser-induced damage threshold, indicating the role the Sc^{3+} cation plays in chalcogenides as a new type of functional NLO gene, which stimulates us to try to introduce Sc to more chalcogenide systems for exploring new multi-functional materials. In fact, Sc-based chalcogenides with birefringence greater than 0.1 have not been reported so far. Even if the scope is expanded to oxides, only two examples, α-$Ba_3Sc_2(BO_3)_4$ [29] and $RbBaScB_6O_{12}$,[30] are available. Compared with other d_0 metal cations, Sc^{3+} is less likely to induce the second-order Jahn–Teller effect, which makes it hard for the ScQ_6 octahedron to undergo significant distortion, subsequently influencing the refractive index and birefringence. There is a possible way to enhance the birefringence performance of Sc-based chalcogenides by modifying the ScQ_6 octahedron with heteroanions. Considering that the polarizability of S is greater than that of O, Sc-based chalcogenides still have the potential to be birefringent materials and achieve a birefringence greater than 0.1. Recent years have witnessed significant advancements in improving optical properties through precise functional group engineering.[31–34] These pioneering studies have significantly informed the design of our Quaternary composite system. Attracted by the rich structures and diverse physical performances of the AM_5Q_8 family, we synthesized a series of quaternary derivatives, *viz.* $NaSc_3Ga_2S_8$ (**1**), $NaSc_3Ga_2Se_8$ (**2**) and $KGa_2In_3S_8$ (**3**), which all crystallize in the CS space group $P\bar{3}m1$ (No. 164). Compared to previous studies, their structures are assembled by MQ_6 and MQ_4 (Q = S, Se) units while retaining 3*D* open channel structures like other AM_5Q_8 compounds. By exploring their structural characteristics, electronic structures, optical properties and potential for optoelectronic applications, it is hoped that useful hints will be obtained for ongoing studies on this amazing family.

Results and discussion

Crystals **1–3** crystallize in the trigonal crystal system with the CS space group $P\bar{3}m1$ (No. 164), representing a new-type structure. Their structures feature a 3*D* open framework $\{[M_5Q_8]^-\}_\infty$ (M = Ga, In and Sc; Q = S and Se), which is constructed by GaQ_4 tetrahedra and MQ_6 octahedra, with A^+ cations located in the cavities of the open channel. Here, the structure of **3** is taken as a representative to describe their structures. In the asymmetric unit, there is one K, one Ga, one In, and two S atoms with full occupancy. Each Ga atom is surrounded by four S atoms to form an isolated GaS_4 tetrahedron, and every In atom is sixfold-coordinated with S atoms to form an InS_6 octahedron (Fig. S5). The distances of the Ga–S and In–S bonds are 2.258(3)–2.299(18) and 2.612(12)–2.665(14) Å, respectively, consistent with those in $Ba_6Zn_7Ga_2S_{16}$,[35] $Ba_8Zn_4Ga_2S_{15}$,[36] $KNa_{0.78}Eu_{0.27}In_{3.80}B_{12}S_{12}$,[37] and $KEu_2In_3B_{12}S_{13}$.[38] The $\{[Ga_3In_2S_8]^-\}_\infty$ anionic framework is

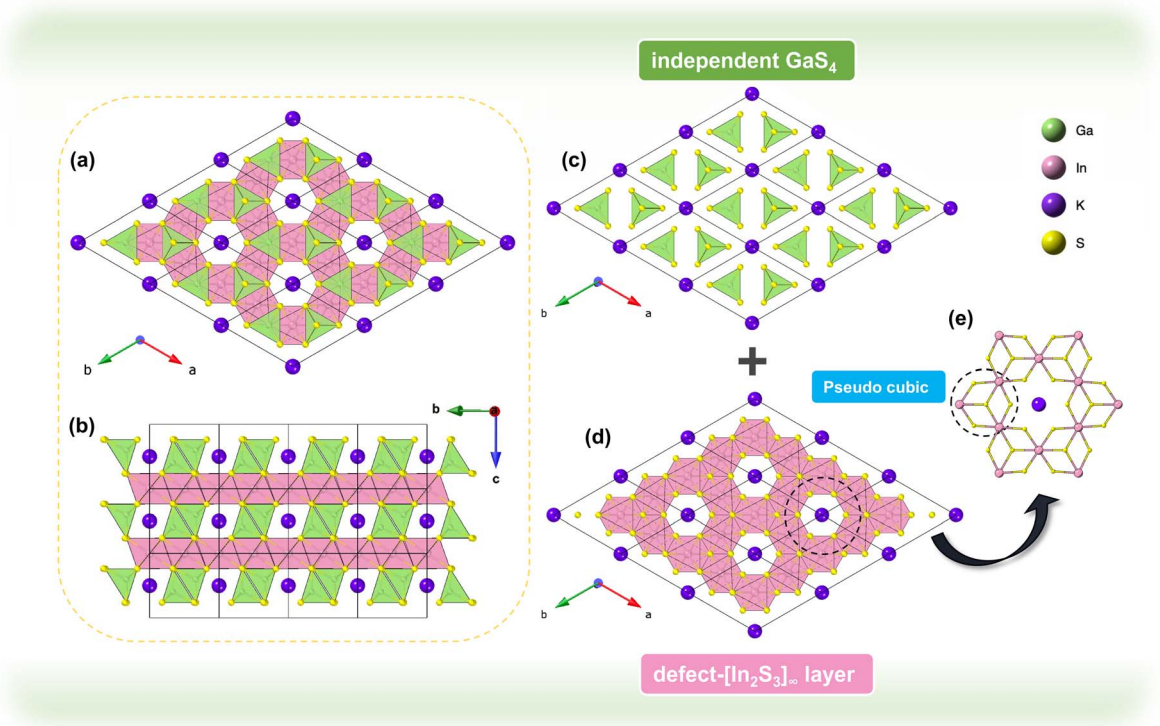

Fig. 1 Observing the crystal structure of **3** along the *c*- (a) and *a*-axis (b), where there are independent GaS_4 tetrahedra and InS_6 octahedra, and the defect-In_3S_4 units constructed layer extending along the *ab* plane. (c) The position of the independent GaS_4 tetrahedra. (d) Defect-In_3S_4 units constructed defect-$[In_2S_3]_\infty$ layer observed along the *c*-axis. (e) $[In_3S_4]$ defect-cubanes form the defect-$[In_2S_3]_\infty$ layer.

composed of $[GaS_4]^{5-}$ tetrahedra and $[InS_6]^{9-}$ octahedra by sharing corners and edges, providing a channel to take up K^+ cations to balance charges and stabilize the structure (Fig. 1a and b). As clearly shown in Fig. 1c, the GaS_4 units extend parallel to the *c*-axis, centro-symmetrically arranged in opposite directions in the *ab*-plane. Individual GaQ_4 (Q = S, Se and Te) tetrahedra are present in chalcogenides but are not widely reported, which appears more in the styles of Ga_xQ_y chains or networks built by corner- or edge-shared GaQ_4 tetrahedra, such as $\{[Ga_6S_{16}]\}_\infty$ chains in β-$BaGa_4S_7$,[39] $[Ga_4S_{14}]$ strings in $Ba_3HgGa_2S_7$,[40] $\{[GaSe_2]^-\}_\infty$ chains in $(Na_{0.60}Ba_{0.70})Ga_2Se_4$,[41] $\{[Ga_8Se_{40/3}]^{(16/3)-}\}_\infty$ layers and $\{[Ga_4Se_{20/3}]^{(8/3)-}\}_\infty$ helical chains in $NaGa_3Se_5$,[42] Ga_2Se_3-like slabs in $KAg_3Ga_8Se_{14}$,[43] and $[Ga_4Q_{11}]$ tetramers in $SnGa_4Q_7$ (Q = S, Se).[44] These crystals possessing 1*D*, 2*D*, and 3*D* secondary structural units formed by GaQ_4 units with shared atoms often exhibit excellent NLO properties.[35,36,45–47] The InS_6 octahedra share the S–S edge and extend along the *ab* plane to form the defect-$[In_2S_3]_\infty$ building layer, which can be considered to be composed of two oppositely arranged $[In_3S_4]$ defect-cubanes with a corner lacking (Fig. 1e). However, the K atom is not located in the center of the cavity formed by defect-In_2S_3 layers (Fig. 1b and d). Similar In–S building layers can be found in $GaInS_3$,[48] but the difference is that there are In atomic vacancies at the 1*a* site. The dipole moments and distortion degrees of InS_6 and ScQ_6 (Q = S, Se) octahedra were calculated. As shown in Table 1, the calculated dipole moment of the InS_6 unit exceeds that of ScQ_6 by several orders of magnitude due to the distortion of InS_6 being much larger than that of ScQ_6, which correlates with the substantially greater octahedral distortion observed in the InS_6 unit. Such remarkable structural distortion in the InS_6 unit induces substantial lattice polarization effects that impact on optical properties. The subsequent content will combine practical characterization and first-principles calculations to state how these structural features affect the light absorption edge and birefringence characteristics.

The IR spectra of **1–3** (Fig. S3) exhibit no distinct peaks over 2.5–25 μm, covering the two important atmospheric IR windows (3–5 and 8–12 μm). The optical band gaps of **1–3** were determined from the UV-vis-NIR diffuse reflectance spectra to be 3.10, 2.21 and 2.85 eV (Fig. S4a–c), respectively. They exhibit an inverse proportionality between their bandgaps and unit cell volumes, where compressive lattice deformation and intensified interatomic interaction may induce bandgap broadening.[27,49,50] For solid-state materials, birefringence Δn is another significant optical property since it can provide valuable information for optoelectronic applications. Due to the fact that **3** is a black crystal, it is difficult to accurately detect the changes in light intensity to measure its birefringence. Therefore, only the birefringences of **1** and **2** were measured at 550 nm, and the values are 0.0437 for **1** and 0.206 for **2**. Fig. S7 shows photographs of **1** and **2** for the birefringence measurement with a polarizing microscope. Meanwhile, the frequency-dependent birefringence Δn values of **1–3** were also calculated (Fig. 2a–c and Table 2), and it can be observed that the birefringence of **3** under three wavelengths of light is more than twice that of **1** and more than one time that of **2**.

The calculated band structures are illustrated in Fig. 2d and e. Compounds **1** and **2** exhibit an indirect bandgap with the valence band maximum (VBM) at the *A* point and the conduction band minimum (CBM) near the *G* point of the first Brillouin zone (BZ), while **3** is a direct bandgap material with its VBM and CBM confined to the *G* point. The computed band gaps of **1–3** are 2.91, 2.29 and 2.39 eV, respectively. The exchange correlation function used in traditional DFT methods has some problems, so there is a significant underestimation of the bandgap when calculating semiconductors.[51] A significant drawback of the mainstream exchange-correlation functionals lies in their failure to effectively correct the self-interaction error (SIE) in the Hartree term. This SIE manifests as a non-physical curvature in the total energy of the system as a function of the number of electrons. Theoretically, there should be a discontinuity in the derivative when the number of electrons is an integer, and a linear relationship when it is a fraction. This error is the main cause of the underestimation of band gaps that is widespread in density functional theory.[52] As shown in Fig. 2g–i, the total density of states (TDOS) and partial density of states (PDOS) of **1–3** are plotted. The VBM of **1** is mainly contributed by the S-3p state, while the CBM is composed of Sc-3d (Fig. 2g). The DOS diagram of **2** is similar to that of **1**, with the VBM mostly given by the Se-4p state and the CBM also consisting of Sc-3d (Fig. 2h). As for **3**, the VBM near the Fermi energy level ($E_f = 0$) is mainly contributed by the S-3p state, while the CBM is mainly composed of In-5s and S-3p orbitals, doped with a small portion of K-3s and Ga-4s orbitals. It should be emphasized that the charge-balanced Na^+ and K^+ cations do not seem to actively participate in the leaps between the VB and CB; the unfilled 3d orbitals of Sc^{3+} cations make a significant contribution in the CB region as compared to In^{3+} in **3**. However, compared with In-4s orbitals, the main contribution region of Sc-3d is further away from E_f, which weakens its contribution to the birefringence in the visible light region. Meanwhile, compared with the strong hybridization effect between In-5s and S-3p orbitals, the low hybridization degree between Sc-3d and S-3p orbitals reduces the strength of the chemical bond, thereby weakening the microscopic anisotropy of the polarizability and the macroscopic birefringence.

Calculation results reveal that the polarizability anisotropy of both GaQ_4 tetrahedra and MQ_6 in **1–3** exhibits a progressive enhancement (Fig. 3), which aligns with the increasing trend of

Table 1 The dipole moments and distortion degrees of the MQ_6 (M = In, Sc; Q = S, Se) octahedra in **1–3**

Unit	Dipole moment/D^a	Distortion $(\Delta d)^b$
ScS_6	5.27×10^{-6}	4.302×10^{-4}
$ScSe_6$	1.041×10^{-5}	2.938×10^{-4}
InS_6	1.241×10^{-3}	6.219×10^{-4}

[a] $\mu = r \times q$ (where q represents the amount of charge and r represents the degree of non-uniformity in charge distribution. The charge of each atom is calculated based on the bond valence model). [b] $\Delta d = \frac{1}{c}\sum[(d_n - d)/d]^2$ (d_n is the single bond length, d is the average bond length, and c is the coordination number.).

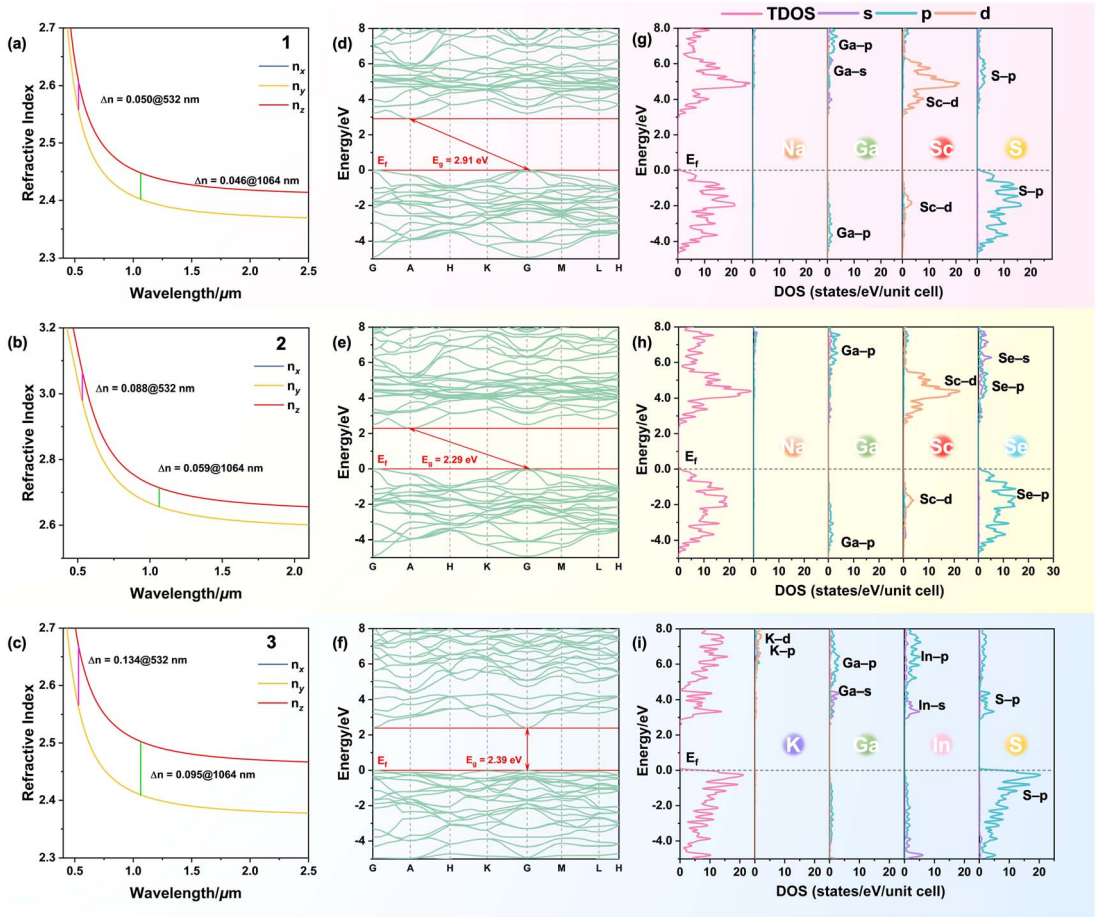

Fig. 2 Theoretical calculations of **1**–**3**. Birefringences at 532 nm and 1064 nm: **1** (a), **2** (b), and **3** (c). Band structures: **1** (d), **2** (e), and **3** (f). TDOS and PDOS curves of **1** (g), **2** (h), and **3** (i). The Fermi level is set at 0 eV.

birefringence.[53] This consistency demonstrates the decisive influence of anisotropic electron cloud distribution in coordination polyhedra on the macroscopic optical anisotropy. The substitution of anions from S to Se leads to a narrowed band gap and increased polarizability, as well as a transition in orbital interaction mode caused by Sc/In cation substitution. This element substitution induced electronic structure change provides a good case for designing novel materials with specific bandgap engineering and large birefringences.

Photocurrent density is directly proportional to the capacity of a material to convert photons into free charge carriers, where higher photocurrent density corresponds to greater electrical energy generation per unit area and enhanced sensitivity to optical signals.[40] The *3D* framework of $\{[Ga_2In_3S_8]^-\}_\infty$ may establish continuous conductive pathways for the rapid transport of carriers. Specifically, The GaS_4 tetrahedra may serve as bridges to facilitate the charge transfer between the adjacent layers, thereby enhancing the overall conductivity. To evaluate these properties, we employed a standard three-electrode system to imitate solar irradiation for a photoelectrochemical

Table 2 Experimental and calculated birefringences of **1**–**3**

	1	**2**	**3**
Experimental birefringence Δ*n*@550 nm	0.044	0.206	—
Theoretical birefringence Δ*n*@532 nm	0.050	0.088	0.134
Theoretical birefringence Δ*n*@1064 nm	0.046	0.059	0.095

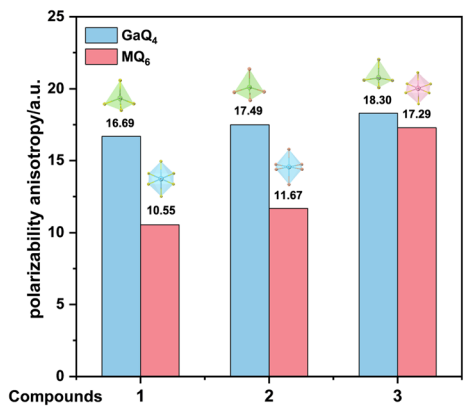

Fig. 3 Polarizability anisotropy of GaQ_4 tetrahedra and MQ_6 (Q = S, Se; M = Sc, In) tetrahedra.

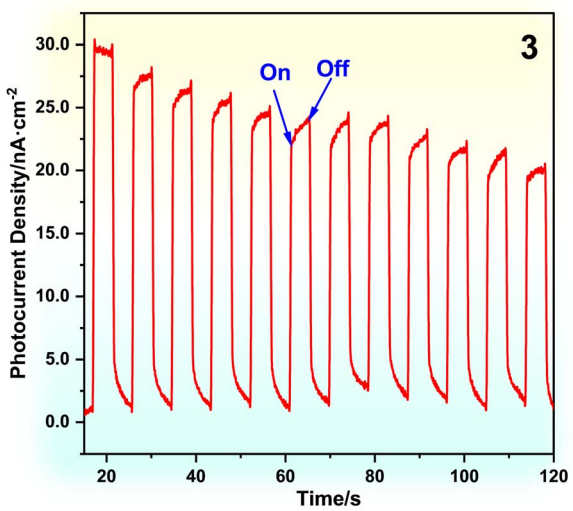

Fig. 4 Photocurrent response curve of **3** (from 15 to 120 seconds).

experiment, and **3** was selected as a representative to study the photoelectric properties. The periodic variation of the photocurrent density under the switching of the light source is shown in Fig. 4. The photocurrent density approaches baseline levels when light is off, while immediate photocurrent is generated upon illumination, indicating the ability of **3** in both effective carrier generation under simulated solar irradiation and fast photoresponse speed. Literature investigation reveals that the photocurrent density of **3** is greater than those of $A_2Ba_3Cu_2Sb_2S_{10}$ (A = K, Rb and Cs, 5∼7 nA cm^{-2}),[54] but still lower than those of some known chalcogenides, such as $Yb_6Ga_4S_{15}$ (∼60 nA cm^{-2}),[55] $AgCdAsS_3$ (0.38 μA cm^{-2}),[56] $Er_4S_4Te_3$ (0.45 μA cm^{-2})[57] and $Ba_3HgGa_2S_7$ (∼12.2 μA cm^{-2}).[40] This may be caused by the fact that **3** has a longer carrier transport path, which increases the probability of carrier recombination, leading to the lower photocurrent density. It may also be possible that the concentration of the suspension sample produced in this experiment is too low (2 mg mL^{-1}), resulting in insufficient light absorption and fewer photogenerated carriers, leading to a lower photocurrent density.[58–60] Photocurrent density decreasing with time is common in chalcogenides.[61] The decrease in photocurrent density of **3** could be attributed to the photo-corrosion phenomenon (chemical degradation or electrode dissolving in electrolyte) during illumination.[62,63] In a previous study, researchers adopted shell coating to effectively solve this problem while improving photocurrent density.[64]

Conclusions

In brief, we report a series of new AM_5Q_8 (A = Na, K; M = Sc, Ga and In; Q = S, Se) chalcogenides crystallizing with a new type of structure. While inheriting the 3*D* open framework from the AM_5Q_8 family, they uniquely incorporate both MQ_4 and MQ_6 motifs. These compounds exhibit wide band gaps, broad infrared transparency window, and pronounced photoelectric response. Specifically, the slight variation in the interaction between metal cations and Q^{2-} anions results in a doubling of the birefringence. This study hopefully provides valuable insights into the design and application of new photoelectronic functional chalcogenide materials.

Author contributions

This work was conceptualised by Y. Xie, W. Zhou and S.-P. Guo. Experimentation was performed by Y. Xie and W.-D. Yao. Software was used by W.-D. Yao and N.-T. Suen. Methodology was performed by Y. Xie and W. Liu. S.-P. Guo. Contributed to funding acquisition and supervision. The first draft of the manuscript was prepared by Y. Xie and W.-D. Yao, and the final draft was edited by all the authors.

Conflicts of interest

The authors declare no competing financial interests.

Data availability

CCDC 2449074−2449076 contain the supplementary crystallographic data for this paper.[65–67]. Data available in the SI includes experimental section, and additional tables and figures. See DOI: https://doi.org/10.1039/d5sc03501e.

Acknowledgements

The authors acknowledge the financial support from the National Natural Science Foundation of China (Grant No. 22371246 and 22401243) and Yunnan Fundamental Research Projects (202401AS070120). W.-D. Yao acknowledges the support by the Postgraduate Research & Practice Innovation Program of Jiangsu Province (KYCX23_3513).

Notes and references

1 K. Wu, Z. Yang and S. Pan, *Angew. Chem., Int. Ed.*, 2016, **55**, 6713–6715.
2 Q. Liu, X. Liu, M. Li, R. Wang, B. Li, L. Wu and L. Chen, *Angew. Chem., Int. Ed.*, 2025, **64**, e202415318.
3 W. van der Stam, A. C. Berends, F. T. Rabouw, T. Willhammar, X. Ke, J. D. Meeldijk, S. Bals and C. de Mello Donega, *Chem. Mater.*, 2015, **27**, 621–628.
4 S. Singh, A. Singh, K. Palaniappan and K. M. Ryan, *Chem. Commun.*, 2013, **49**, 10293–10295.
5 S.-M. Pei, M.-S. Zhang, F. Wu, Y. Guo, X.-M. Jiang, B.-W. Liu and G.-C. Guo, *Chem. Sci.*, 2024, **15**, 13753–13759.
6 S. Yang, X. Xu, Y. Zhu, R. Niu, C. Xu, Y. Peng, X. Cheng, X. Jia, Y. Huang, X. Xu, J. Lu and Y. Ye, *Phys. Rev. X*, 2021, **11**, 011003.
7 H. L. Zhuang, Y. Xie, P. R. C. Kent and P. Ganesh, *Phys. Rev. B:Condens. Matter Mater. Phys.*, 2015, **92**, 035407.
8 H. Bouteiller, B. Fontaine, O. Perez, S. Hébert, C. Bourgès, Y. Matsushita, T. Mori, F. Gascoin, J.-F. Halet and D. Berthebaud, *Inorg. Chem.*, 2024, **63**, 16655–16666.

9 A. I. Romanenko, G. E. Chebanova, T. Chen, W. Su and H. Wang, *J. Phys. D: Appl. Phys.*, 2021, **55**, 143001.
10 S. Hébert, R. Daou, A. Maignan, S. Das, A. Banerjee, Y. Klein, C. Bourgès, N. Tsujii and T. Mori, *Sci. Technol. Adv. Mater.*, 2021, **22**, 583–596.
11 Q. Si, R. Yu and E. Abrahams, *Nat. Rev. Mater.*, 2016, **1**, 16017.
12 N. C. Gresty, Y. Takabayashi, A. Y. Ganin, M. T. McDonald, J. B. Claridge, D. Giap, Y. Mizuguchi, Y. Takano, T. Kagayama, Y. Ohishi, M. Takata, M. J. Rosseinsky, S. Margadonna and K. Prassides, *J. Am. Chem. Soc.*, 2009, **131**, 16944–16952.
13 S.-C. Zhu and F.-X. Xiao, *ACS Catal.*, 2023, **13**, 7269–7309.
14 N. Kapuria, S. Imtiaz, A. Sankaran, H. Geaney, T. Kennedy, S. Singh and K. M. Ryan, *Nano Lett.*, 2022, **22**, 10120–10127.
15 S. Yamazaki and Y. Ueda, *Solid State Phenom.*, 2011, **170**, 17–20.
16 J. Babo and T. Schleid, *Z. Anorg. Allg. Chem.*, 2008, **634**, 1463–1465.
17 D. L. Gray and J. A. Ibers, *J. Alloys Compd.*, 2007, **440**, 74–77.
18 L. Fournès, M. Vlasse and M. Saux, *Mater. Res. Bull.*, 1977, **12**, 1–5.
19 P. Tumurugoti, S. Betal and S. K. Sundaram, *Int. Mater. Rev.*, 2021, **66**, 141–159.
20 F. Boucher, J. Gareh, O. Gourdon, M. Evain and C. J. O'Connor, *J. Solid State Chem.*, 1997, **131**, 326–334.
21 H. Bouteiller, B. Fontaine, T. Mori, F. Gascoin, J.-F. Halet and D. Berthebaud, *Inorg. Chem.*, 2023, **62**, 16905–16912.
22 S. Maier, R. Lefèvre, X. Lin, R. Nunna, D. Berthebaud, S. Hèbert, A. Mar and F. Gascoin, *J. Mater. Chem. C*, 2015, **3**, 10509–10517.
23 L. Dong, S. Zhang, P. Gong, F. Liang and Z. Lin, *Inorg. Chem. Front.*, 2023, **10**, 3248–3254.
24 W.-F. Chen, X.-M. Jiang, S.-M. Pei, M.-S. Zhang, B.-W. Liu and G.-C. Guo, *Sci. China Mater.*, 2023, **66**, 740–747.
25 M.-X. Li, Y. Guo, M.-N. Jing, M.-K. Gao, X.-M. Jiang, B.-W. Liu and G.-C. Guo, *ACS Appl. Mater. Interfaces*, 2025, **17**, 14250–14256.
26 H. Lee, B. Yoo, D. Kim, J. Cha, Y. K. Kang, S.-P. Cho, T. Hyeon, M.-G. Kim, M. G. Kanatzidis and I. Chung, *J. Am. Chem. Soc.*, 2023, **145**, 15951–15962.
27 W.-F. Chen, B.-W. Liu, S.-M. Pei, Q.-N. Yan, X.-M. Jiang and G.-C. Guo, *Chem. Mater.*, 2021, **33**, 3729–3735.
28 C.-Y. Zhao, C.-L. Hu, N.-T. Suen, X.-H. Li, H.-P. Xu, W. Zhou and S.-P. Guo, *Adv. Sci.*, 2025, **12**, e2411960.
29 J. Zhou, P. Gong, M. Xia, A. Ji, L. Zhang, H. Wu and Q. Wu, *Inorg. Chem.*, 2023, **62**, 8931–8939.
30 W. Liu, P. Gong, W. Huang, M. Sun, S. Zhao, Z. Lin and J. Yao, *Inorg. Chem.*, 2023, **62**, 10461–10469.
31 X. Dong, L. Huang, C. Hu, H. Zeng, Z. Lin, X. Wang, K. M. Ok and G. Zou, *Angew. Chem., Int. Ed.*, 2019, **58**, 6528–6534.
32 Y. Deng, L. Huang, X. Dong, L. Wang, K. M. Ok, H. Zeng, Z. Lin and G. Zou, *Angew. Chem., Int. Ed.*, 2020, **59**, 21151–21156.
33 Y. Tian, W. Zeng, X. Dong, L. Huang, Y. Zhou, H. Zeng, Z. Lin and G. Zou, *Angew. Chem., Int. Ed.*, 2024, **63**, e202409093.
34 X. Dong, L. Huang and G. Zou, *Acc. Chem. Res.*, 2025, **58**, 150–162.
35 Y.-Y. Li, P.-F. Liu and L.-M. Wu, *Chem. Mater.*, 2017, **29**, 5259–5266.
36 Y.-Y. Li, P.-F. Liu, H. Lin, L.-M. Wu, X.-T. Wu and Q.-L. Zhu, *Chem. Commun.*, 2019, **55**, 7942–7945.
37 S.-S. Han, S.-X. Yu, W. Liu and S.-P. Guo, *Inorg. Chem. Front.*, 2022, **9**, 2462–2469.
38 S.-S. Han, Q.-T. Xu, W. Liu and S.-P. Guo, *Dalton Trans.*, 2022, **51**, 4619–4622.
39 Z. Qian, H. Liu, Y. Zhang, H. Wu, Z. Hu, J. Wang, Y. Wu and H. Yu, *Inorg. Chem. Front.*, 2022, **9**, 4632–4641.
40 X. Huang, S.-H. Yang, W. Liu and S.-P. Guo, *Inorg. Chem.*, 2022, **61**, 12954–12958.
41 Y.-N. Li, H. Xue and S.-P. Guo, *Inorg. Chem.*, 2020, **59**, 3546–3550.
42 Q.-T. Xu, S.-S. Han, J.-N. Li and S.-P. Guo, *Inorg. Chem.*, 2022, **61**, 5479–5483.
43 J.-N. Li, W.-D. Yao, X.-H. Li, W. Liu, H.-G. Xue and S.-P. Guo, *Chem. Commun.*, 2021, **57**, 1109–1112.
44 Z.-Z. Luo, C.-S. Lin, H.-H. Cui, W.-L. Zhang, H. Zhang, Z.-Z. He and W.-D. Cheng, *Chem. Mater.*, 2014, **26**, 2743–2749.
45 L. Luo, L. Wang, J. Chen, J. Zhou, Z. Yang, S. Pan and J. Li, *J. Am. Chem. Soc.*, 2022, **144**, 21916–21925.
46 X. Lin, G. Zhang and N. Ye, *Cryst. Growth Des.*, 2009, **9**, 1186–1189.
47 M.-M. Chen, S.-H. Zhou, W. Wei, X.-T. Wu, H. Lin and Q.-L. Zhu, *Inorg. Chem.*, 2021, **60**, 10038–10046.
48 T. V. Vu, N. N. Hieu, A. A. Lavrentyev, O. Y. Khyzhun, C. V. Lanh, A. I. Kartamyshev, H. V. Phuc and N. V. Hieu, *RSC Adv.*, 2022, **12**, 7973–7979.
49 L. C. Tang, M. H. Lee, C. H. Yang, J. Y. Huang and C. S. Chang, *J. Phys.: Condens. Matter*, 2003, **15**, 6043.
50 J. Li, W.-D. Yao, J.-N. Li, X.-H. Li, W. Liu and S.-P. Guo, *Mater. Today Phys.*, 2023, **32**, 101007.
51 B. Almoussawi, W.-D. Yao, S.-P. Guo, M.-H. Whangbo, V. Dupray, S. Clevers, S. Deng and H. Kabbour, *Chem. Mater.*, 2022, **34**, 4375–4383.
52 E. B. Linscott, D. J. Cole, M. C. Payne and D. D. O'Regan, *Phys. Rev. B*, 2018, **98**, 235157.
53 T. Lu and F. Chen, *J. Comput. Chem.*, 2012, **33**, 580–592.
54 C. Liu, Y. Xiao, H. Wang, W. Chai, X. Liu, D. Yan, H. Lin and Y. Liu, *Inorg. Chem.*, 2020, **59**, 1577–1581.
55 H. Lin, J.-N. Shen, W.-W. Zhu, Y. Liu, X.-T. Wu, Q.-L. Zhu and L.-M. Wu, *Dalton Trans.*, 2017, **46**, 13731–13738.
56 J. Tang, F. Liang, W. Xing, C. Tang, W. Yin, B. Kang and J. Deng, *Inorg. Chem.*, 2023, **62**, 14739–14747.
57 Y. Chi, L.-Z. Rong, N.-T. Suen, H.-G. Xue and S.-P. Guo, *Inorg. Chem.*, 2018, **57**, 5343–5351.
58 Y. Yu, L. Gao, X. Niu, K. Liu, R. Li, D. Yang, H. Zeng, H.-Q. Wang, Z. Ni and J. Lu, *Adv. Mater.*, 2023, **35**, 2210157.
59 S. V. Novikov, *Russ. J. Electrochem.*, 2024, **60**, 904–912.
60 Z. He, R. Yu, Y. Dong, R. Wang, Y. Zhang and Z. Tan, *Nat. Commun.*, 2025, **16**, 1773.
61 Y. Xiao, S.-H. Zhou, R. Yu, Y. Shen, Z. Ma, H. Lin and Y. Liu, *Inorg. Chem.*, 2021, **60**, 9263–9267.

62 B. Weng, M.-Y. Qi, C. Han, Z.-R. Tang and Y.-J. Xu, *ACS Catal.*, 2019, **9**, 4642–4687.
63 S. Al Bacha, S. Saitzek, H. Kabbour and E. E. McCabe, *Inorg. Chem.*, 2024, **63**, 3292–3302.
64 B. Tian, W. Gao, X. Zhang, Y. Wu and G. Lu, *Appl. Catal., B*, 2018, **221**, 618–625.
65 Y. Xie, W.-D. Yao, Q.-Y. Du, W. Zhou, N.-T. Suen, W. Liu and S.-P. Guo, CCDC 2449074: Experimental Crystal Structure Determination, 2025, DOI: **10.5517/ccdc.csd.cc2n6gdr**.
66 Y. Xie, W.-D. Yao, Q.-Y. Du, W. Zhou, N.-T. Suen, W. Liu and S.-P. Guo, CCDC 2449075: Experimental Crystal Structure Determination, 2025, DOI: **10.5517/ccdc.csd.cc2n6gfs**.
67 Y. Xie, W.-D. Yao, Q.-Y. Du, W. Zhou, N.-T. Suen, W. Liu and S.-P. Guo, CCDC 2449076: Experimental Crystal Structure Determination, 2025, DOI: **10.5517/ccdc.csd.cc2n6ggt**.